

# First-order theories for adiabatic $L$ -shell ionization by protons

Ž. Šmit\* and I. Orlić

*Department of Physics, National University of Singapore, Singapore 0511, Singapore*

(Received 24 March 1994)

$L$ -shell ionization cross sections, evaluated as mean values of the experimental data, were compared with the first-order theoretical values obtained by the plane-wave Born and semiclassical method. Hydrogenic Dirac wave functions in the united-atom limit were employed in the calculation. The plane-wave Born approximation cross sections with Dirac-Hartree-Slater wave functions were obtained from the tables of Chen and Crasemann [At. Data Nucl. Data Tables **33**, 217 (1985); **41**, 257 (1989)]. The agreement between the experimental and semiclassical cross sections was generally better than 20%, except for the  $L_1$  subshell of heavy elements and for the very adiabatic region of  $L_{2,3}$  subshells. The differences between both sets of data were largely reproduced by a simplified coupled-channel calculation performed nonrelativistically for a single final state. The calculation also suggests that, due to the uncertainties of the fluorescence yields, the ionization cross sections deduced from the measured data are overestimated by 10%.

PACS number(s): 34.10.+x, 34.50.Fa, 03.65.Sq

## I. INTRODUCTION

A comprehensive statistical evaluation of the  $L$ -shell ionization cross sections, performed at the National University of Singapore during recent years, provides a data base which can be effectively used for studies of the  $L$ -shell cross sections within an accuracy of a few percent [1,2]. As most of the experimental data have been obtained by x-ray spectroscopy using semiconductor detectors which are inefficient in the sub-keV region, the majority of the data are for heavier elements,  $Z_2 \gtrsim 40$ . For proton bombardment, the atomic number ratio  $Z_1/Z_2 \lesssim 0.025$  is then sufficiently small for the first order theories to yield reliable results. Indeed, the perturbed-stationary-state (PSS) theory with energy-loss (E), Coulomb deflection (C), and relativistic (R) correction (ECPSSR) [3] agrees with the experimental data within a factor of 2 in a rather broad energy and  $Z_2$  interval [2]. The ECPSSR cross sections can be easily calculated and have been widely used for the normalization of experimental data in the statistical procedures [2,4]. However, it is known from the studies of the  $K$ -shell ionization process that the Coulomb correction used in the model [3] is underestimated in the very adiabatic region [5]. Furthermore, the binding correction takes into account only the change of the binding energy due to the presence of the charged projectile, neglecting the change of the wave function. In the adiabatic region, the binding correction underestimates the cross section. The relativistic correction [3] increases the cross sections for non-relativistic wave functions more than the corresponding use of the Dirac wave functions [6].

The corrections introduced by the ECPSSR theory [3] are not independent. Their deficiencies partly compensate each other for certain projectile velocities. It is therefore futile to inspect or revise them individually. No relativistic corrections are necessary when Dirac wave functions are used. Within the semiclassical approach, the Coulomb trajectory of the projectile is explicitly taken into account. It is then the binding effect alone which limits the validity of first-order models. In further analysis we shall restrict ourselves to sufficiently slow collisions, characterized by the reduced velocity parameter  $\xi$  [7] smaller than unity. In this region the change of the electron binding energy and of the wave function is ingeniously taken into account by the united-atom model [8], where the ionization process occurs in a virtual atom of the atomic number  $Z_1 + Z_2$ . In subsequent refinements of the united-atom model for the  $K$ -shell [9,10], a generally better agreement with the experiment was not found. This can be explained by an unrealistic proposition that the electron wave functions adjust instantly to the position of the projectile. The importance of the wave function time evolution is clearly demonstrated observing the transitions in a harmonic oscillator perturbed by a time dependent coupling of an additional spring [11]. The united-atom case corresponds to the oscillator with the perturbing spring coupled permanently. The transition probabilities for the "united-atom" type of the wave functions differed significantly from the results obtained by the coupled-channel method.

There are no straightforward binding correction procedures between the calculations in the united-atom model or those for the more elaborate coupled-channel approach. We shall therefore adopt the united-atom model for our first order calculations. For  $L$ -shells, the united-atom binding procedure has already been used in the very adiabatic region by Vigilante *et al.* [12].

It is significant that for the  $L$ -shell ionization the per-

---

\*Permanent address: J. Stefan Institute, University of Ljubljana, Ljubljana, Slovenia.

turbing field of the projectile induces redistribution of vacancies among different  $L$ -subshells [13]. The deficiency of the first order models on account of this effect will be studied by a simplified coupled-channel approach.

## II. THEORETICAL MODELS

In a multielectron atom, the adequate inner shell wave functions are of the Dirac-Hartree-Slater type, which were used by Chen and Crasemann for the cross-section calculation in the plane-wave approximation [14]. For the semiclassical approach which describes the ionization process to greater detail, we used the hydrogenic atomic model. The wave functions used were screened hydrogenic Dirac wave functions, where the screening due to inner electrons was taken into account according to Slater, and that due to outer electrons according to Bethe [15]. If the energy of the projectile transferred to the electron is close to the binding energy, the electron transits not to the continuum but to a virtually bound state. The missing energy is supplied in a later stage of the collision on account of shrinking of the electron cloud.

In order to investigate the differences in cross sections obtained by different wave functions, we first calculated the cross sections in the relativistic plane-wave Born approximation (RPWBA) with screened Dirac hydrogenic wave functions. The functions were then used in the semiclassical calculations for which we developed a new computer code. The semiclassical calculations were also performed by the code IONHYD of Trautmann and Rösel [16] which differs from the present one in its specific hydrogenic approximation.

The principle of Bethe was generally used in plane-wave methods, but not in the semiclassical ones. Since both methods yield the same results for energetic projectiles whose trajectories approach straight lines, this criterion provided an essential test for the numerical accuracy of our calculations.

### A. Dirac-Hartree-Slater cross sections

RPWBA cross sections using Dirac-Hartree-Slater (DHS) wave functions [14] are tabulated for selected elements in three forms: the uncorrected cross sections, the cross sections corrected for the binding effect according to [3], and the cross sections corrected both for the binding and Coulomb effect. Since the united-atom approach was used throughout our calculations, the united-atom DHS cross sections were taken to be the uncorrected values of the neighboring  $Z_2 + Z_1$  element. The errors introduced using this procedure are a slightly overestimated reduced mass of the projectile and an additional electron in the outer shells. For  $Z_2 \gtrsim 40$  elements, both effects were estimated to contribute negligibly to the ionization cross sections. For a selected element and proton energy, the cross-section values were obtained by interpolation from tables. The interpolated quantity was the ratio between the tabulated cross sections and the nonrelativistic PWBA values, which deviates from unity by less than a factor of 2. The deduced cross sections were then mul-

tiplied by the Coulomb correction factors of the original element.

### B. RPWBA cross sections

The plane-wave cross sections for hydrogenic Dirac wave functions were obtained from the standard expression [17,18]

$$\sigma = 8\pi Z_1^2 \alpha^2 \left(\frac{c}{v}\right)^2 \int dW \int \frac{2dq}{q^3} |F_{L_i}(q)|^2, \quad (1)$$

where  $\mathbf{q}$  and  $W$  are the momentum and energy transferred to the atomic electron, respectively,  $v$  the velocity of the projectile,  $c$  the velocity of light, and  $\alpha$  the fine structure constant. Using the results of the angular integrations [18], the square of the electron form factor  $F_{L_i}(q)$  may be written as

$$|F_{L_1}(q)|^2 = \sum_{l=0, \kappa=-l-1, l} |\kappa| [J_{L_1, \kappa}^l(q)]^2,$$

$$|F_{L_2}(q)|^2 = \sum_{l=0, \kappa=-l-1, l} |\kappa| [J_{L_2, \kappa}^{\{l+1, l-1\}}(q)]^2,$$

$$|F_{L_3}(q)|^2 = \sum_{l=0, \kappa=-l-1, l} \{1, 3\} \frac{|\kappa|(|\kappa| - 1)}{2l + 1} [J_{L_3, \kappa}^{l-1}(q)]^2 + \{3, 1\} \frac{|\kappa|(|\kappa| + 1)}{2l + 1} [J_{L_3, \kappa}^{l+1}(q)]^2, \quad (2)$$

where the first value in the curly brackets refers to  $\kappa = -l - 1$  and the second one to  $\kappa = l$ . The radial integrations are contained in the expression

$$J_{L_i, \kappa}^l(q) = \int j_l(qr) [g_\kappa(r)g_{L_i}(r) + f_\kappa(r)f_{L_i}(r)] r^2 dr, \quad (3)$$

where  $g$  and  $f$  are the large and small components of the Dirac wave function for the initial and final state, respectively. The integration (3) was performed numerically by the transformation procedure according to Talman [19], and the continuum wave functions were generated by the step-controlled Runge-Kutta procedure from the analytic expansion of the Dirac wave functions at small  $r$  [5]. Partial waves up to  $l = 5$  were included in the calculation and the numerical accuracy was maintained within 1%.

### C. Semiclassical cross section

In the semiclassical approximation, the separation of projectile and electron variables is generally performed either in the momentum or in the coordinate space [20]. The momentum space method was used for our  $K$ -shell calculation [5] and the existing program can easily be modified for the  $L_1$ -shell ionization. However, the coupled-channel calculations stimulated the development

of a code which was based on the coordinate method. Expanding the electron functions in the orthonormal set of atomic eigenstates

$$\Psi = \sum_n a_n(t) |n\rangle e^{i\omega_n t} \quad (4)$$

we obtain a set of coupled equations

$$\begin{aligned} \frac{d a_f}{ds} = & -i Z_1 \alpha \frac{c}{v} \sum_n a_n \left\langle f \left| \frac{1}{|\mathbf{R} - \mathbf{r}|} \right| n \right\rangle \\ & \times \exp \left( i \frac{\omega_f - \omega_n}{v} s \right), \end{aligned} \quad (5)$$

where  $\mathbf{R}$  and  $\mathbf{r}$  denote the projectile and electron position vector, respectively. We also introduced the variable  $s = vt$ . In the first-order approximation,  $a_0 = 1$ ,  $a_{n>0} = 0$ , and the summation  $n$  reduces to the  $n = 0$  term. The ionization cross section is given by

$$\sigma = \int dW \int |a_f(W)|^2 2\pi b db. \quad (6)$$

By multipole expansion of  $\frac{1}{|\mathbf{R} - \mathbf{r}|}$ , the radial dependence of the matrix elements in (5) is given by the functions

$$\begin{aligned} G_l(R) = & \frac{1}{R^{l+1}} \int_0^R (g_\kappa g_{L_i} + f_\kappa f_{L_i}) r^{l+2} dr \\ & + R^l \int_R^\infty (g_\kappa g_{L_i} + f_\kappa f_{L_i}) r^{1-l} dr. \end{aligned} \quad (7)$$

For  $l = 1$ ,  $G_1(R)$  is increased by the recoil contribution [21]

$$G_1^{\text{rec}}(R) = Z_2 \frac{m}{M_2} \frac{E_i + E_f}{2m c^2} \frac{\langle r \rangle}{R^2}, \quad (8)$$

where  $m$  is the electron mass,  $\langle r \rangle$  the matrix element of the electron dipole operator, and  $E_i$  and  $E_f$  are the electron initial and final energy with  $m c^2$  offset, respectively.

For Coulomb trajectories we used a parametric representation of the hyperbola which is approximately linear for large projectile-target nucleus distances [11]. The inelasticity of the collision was taken into account by the procedure [22] which replaces  $1/v^2$  by its symmetrized value  $1/vv'$ ,  $v'$  being the projectile velocity after the collision. In (5), the symmetrized value of  $1/vv'$  has a noticeable effect only on the exponential function. Within a linear approximation, this correction is equivalent to assuming in (5) a realistic value of the minimum momentum transfer  $\Delta\omega/v$ .

For the first-order integration of (5) we used the method of Ford *et al.* [23], generalized to the fourth-order polynomial. For very adiabatic collisions, the algorithm was optimized to avoid an unnecessary summation of positive and negative numbers. The functions  $G_l$  were precalculated for a set of  $R$  values spaced logarithmically, and the necessary values of  $G_l$  were obtained by a rational function interpolation. For sufficiently large values of  $R$ , the second integral in (7) was regarded as negligibly small, and the values of  $G_l$  were obtained by scaling in  $R^{l+1}$ . The integration procedure in (7) was Gaussian,

and by careful bookkeeping, the continuum wave functions had to be computed only once for a particular final state energy.

The calculation included continuum states up to  $l = 2$ . For  $\xi \lesssim 1$ , the higher multipole states contribute less than 10% to the total cross sections. Since this contribution originates from large impact parameters, it is a good approximation to calculate it in a straight line limit. This is equivalent to the plane-wave approximation and we have adopted it for the partial cross sections of  $l > 2$ .

The accuracy of the calculation was within 1%, as checked by comparing the results for  $K$  and  $L_1$  shells, obtained by the present coordinate and momentum space [5] methods. The same accuracy was estimated also for the values of  $\xi$  close to unity, where the contribution of higher multipole states becomes noticeable.

#### D. Coupled-channel calculations

It is expected that the coupled-channel model yields a more accurate description of the binding effect and estimates the contribution of the projectile induced vacancy redistribution among different subshells [13]. The calculations performed here were of the simplest nonrelativistic type and primarily intended to demonstrate the validity of the first-order theories. Several approximations were introduced.

(a) Numerical solution of the system (5) can only be performed for a finite number of states. A realistic cutoff depends on the size of the perturbation, i.e., on the  $Z_1/Z_2$  ratio. Trial calculations using the analogous harmonic oscillator model [11] showed that, within a few percent accuracy, only the two lowest states may be used for the perturbation corresponding to  $Z_1/Z_2 < 0.025$ . The  $L$ -shell calculation may therefore be limited to a few lowest states.

(b) We have assumed that the continuum consists of only one state, similar to the model [13]. The results of the coupled-channel calculation are then reported as a ratio to the respective first-order values. In our case, these are given by the first-order solution (5) in the united-atom limit.

(c) The choice of the continuum state is not unique. In the approach of Sarkadi and Mukoyama [13, 24–26], a collision with minimum energy transfer results in an electron transition to the lowest continuum state with zero energy. This principle is contradictory to that of Bethe, where the lowest final states are virtually bound. Since the three subshells have different binding energies, the corresponding lowest final states are described by different wave functions. It seems that strict validity of Bethe's principle is questionable in the  $L$ -shell case since only a large part of the  $L_1$ - $L_2$  energy difference can be explained by screening due to other electrons [27], while the  $L_2$ - $L_3$  energy difference is mainly due to  $LS$  coupling. We have therefore used the following procedure, which is specific for our calculation. The lowest final state was determined from the mean  $L$ -shell binding energy. For the examples shown below, the final state was between the states of  $n = 3$  and  $n = 4$ . As a further approxi-

mation we chose the transitions into the  $n = 4$  state as most representative. In order to estimate the variation of our results with  $n$ , the calculation was also performed for the  $n = 3$  final state. The choice of the  $n = 4$  case is physically more sound since its energy transfer, which exceeds the minimum one, approaches the mean energy transfer in the ionizing collision. By using an integer  $n$  for the final state, the matrix elements in (5) reduce to close analytical expressions which considerably facilitate the solution of the system of coupled equations. Furthermore, it is possible to explicitly include the coupling of the final state to itself.

(d) The system (5) was solved for a deexcitation process which is roughly similar to the transitions of vacancies in the relativistic calculations [28,29]. An electron was initially set into one of the  $4s, p$  states and the transitions into the bound  $L$  states were observed. No  $LS$  coupling was considered in the  $4s, p$  state. Since the results have to be independent of the initial choice of the electron spin, we used this effect as a general check for our procedure. The backcoupling bound state continuum was omitted in (5), but we included all diagonal terms. For the calculation of  $L$ - $L$  matrix elements, the results of [30,31] were indispensable. The numerical procedure for solving (5) was of a modified midpoint type extrapolating the step size to zero [32]. As the transitions of vacancies between different  $L$  subshells depend strongly on the impact parameter [29], the integration for the impact parameter in (6) was carried out. The algorithm was a simple fifth-order Gaussian, and the final result was the ratio between the coupled-channel cross section and that for the united-atom.

### III. EXPERIMENTAL CROSS SECTIONS

The theoretical values were compared to the experimental data from the compilation [1]. The averaging procedure of the experimental data [33,34] was similar to that for the  $K$  shell [4], but using a different rejection method. The procedure included the newly compiled data, so there were generally 1700 experimental points per subshell. The experimental points were normalized to the ECPSSR cross sections, and grouped in equidistant intervals of the variable  $\log \xi$ . The mean values of each interval yielded the so called “ $s$  functions” [4]. As the  $Z_2$  dependence of the ECPSSR cross sections is not entirely correct, the elements were divided into three independent groups. The points which differed by a certain value from the mean were rejected, and the new mean value was sought. The difference between the two sets of the mean values was generally on a percent level, except in the very adiabatic region [34].

The  $s$  functions were also used to generate reference experimental cross sections. The procedure is most accurate for the elements which are in the middle of the  $Z_2$  intervals. This implied the choice of Sn, Dy, and Pb for the representative elements. The errors in the cross section are then essentially determined by the statistical distribution of the measured points.

### IV. DISCUSSION

As mentioned before, the first-order theories involved in the present analysis were RPWBA with DHS wave functions [14], RPWBA with screened hydrogenic Dirac wave functions, and the semiclassical approximation (SCA) as evaluated by the code IONHYD [16] and that by the present authors. It should be kept in mind that the united-atom binding procedure was used systematically.

The ratios between the experimental and both types of the RPWBA cross sections are shown in Figs. 1 and 2. For  $L_{2,3}$  subshells, the experimental and calculated cross sections agree within 20% for moderately low velocities. For  $\xi < 0.4$ , the ratios of the experimental to theoretical cross sections show a rapid decrease which indicates the inefficiency of the approximate Coulomb correction factor [3]. The  $L_1$  experimental cross sections exceed the RPWBA values by up to 40% and the corresponding breakdown of the Coulomb correction at low  $\xi$  is not so apparent. Figures 1 and 2 also enable us to study the effect of using a different type of wave functions in the calculation. The cross-section ratios obtained by the DHS and hydrogenic wave functions generally differ by

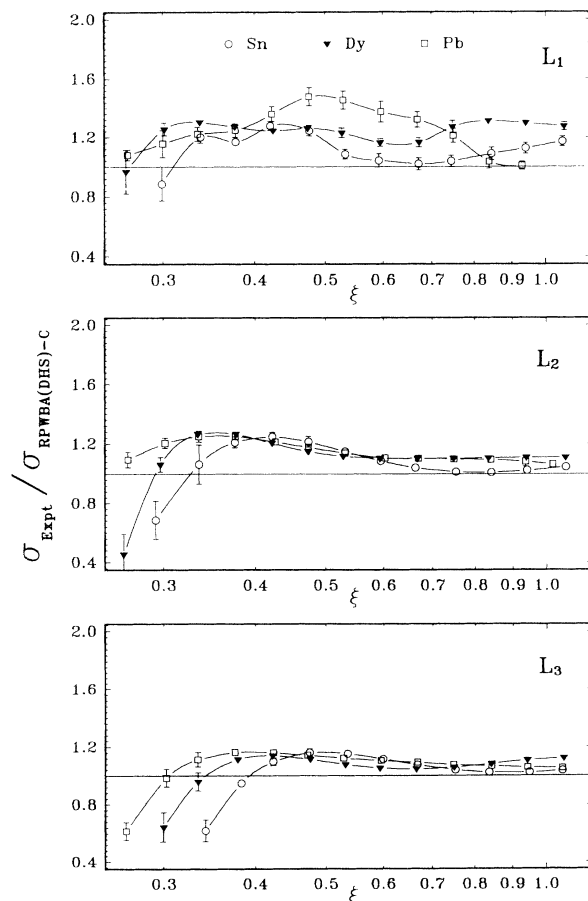


FIG. 1. The ratios between the average experimental and RPWBA cross sections using DHS wave functions in the united-atom limit [14].

less than 10%, except for the  $L_1$  subshell where the differences amount to up to 20%. This can be explained by the node of the  $L_1$  wave function which has a marked effect on the size of the cross section.

A more realistic cross section ratio for  $\xi < 0.4$  is obtained by a semiclassical approach. Figures 3 and 4 show the ratio between the experimental and semiclassical cross sections, calculated by the method of [16] and the present one, respectively. For  $\xi \gtrsim 0.7$ , the Coulomb correction factor [3] is greater than 0.9 and we expect that the ratios in Figs. 3 and 4 approach the corresponding ratios obtained by the RPWBA methods. This is indeed the case for the present calculation shown in Fig. 4, while the ratios in Fig. 3 calculated by the method of [16] are lower by between 20% and 40%. We may conjecture that this difference is due to the specific hydrogenic approximation used by the authors [16] which differs from that using the principle of Bethe. However, the use of the principle of Bethe is strongly supported by the good agreement between the present hydrogenic and DHS cross sections.

We shall next compare the results of Fig. 4 to those of the coupled-channel calculations (Fig. 5). It is first observed that the choice of using either the  $4s, p$  or the

$3s, p$  wave function for the representative final state does not significantly alter the shape of the cross section ratios in Fig. 5, though the position along the  $\xi$  axis may vary up to  $\Delta\xi \sim 0.1$ .

We may expect that the structures in the ratio between the experimental and semiclassical united-atom cross sections (Fig. 4) are reflected in the corresponding ratio between the coupled-channel and united-atom cross sections of Fig. 5. For the  $L_1$  calculation in Fig. 5, a common feature is a broad dip at  $\xi \sim 0.5$ . This dip may be traced for Sn and Dy data in Fig. 4, while Pb data for  $\xi > 0.5$  behave in a completely different way, showing a maximum at  $\xi \sim 0.6$ . The occurrence of this maximum cannot be explained.

The cross section ratios for the  $L_2$  subshell in Fig. 5 largely exceed unity for the adiabatic collisions  $\xi < 0.4$ , as already pointed out by Sarkadi for helium projectiles [24] and by Vigilante and co-workers [12,35] for the case of protons. For  $\xi \lesssim 0.4$ , smooth maxima tend to appear in the cross-section ratios of Fig. 4. The intensities of these maxima increase with increasing  $Z_2$ , and their positions shift to the lower values of  $\xi$ . There is a similar trend in the data obtained by the coupled-channel calculation (Fig. 5), except that the intensities of the maxima

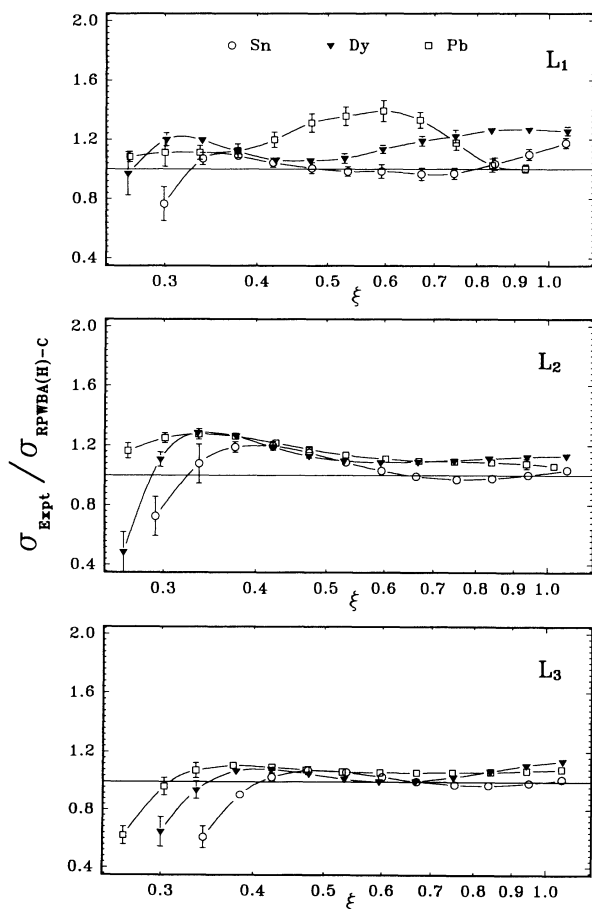


FIG. 2. The ratios between the average experimental and RPWBA cross sections obtained by the hydrogenic Dirac wave functions.

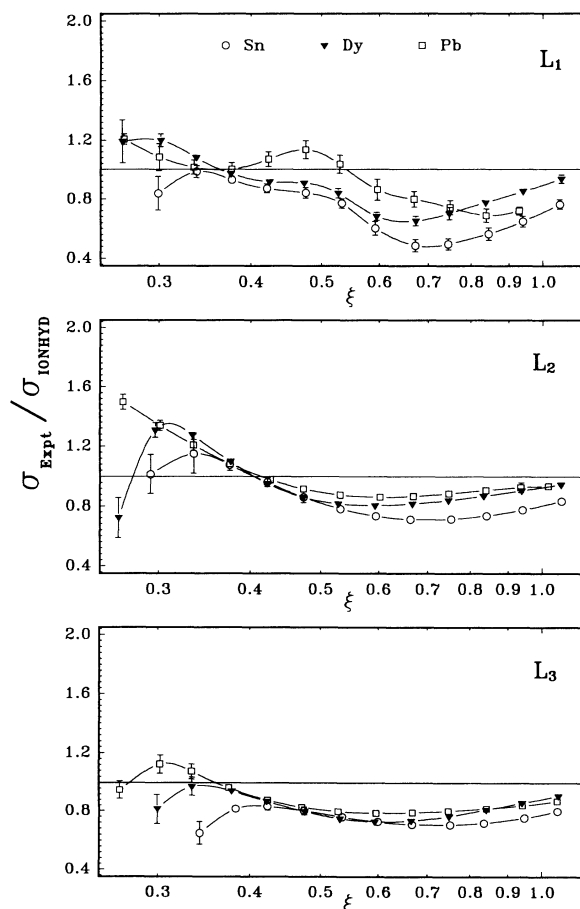


FIG. 3. The ratios between the average experimental and semiclassical cross sections calculated by the code IONHYD [16].

are lower and their positions are shifted to values of  $\xi$  which are lower by 0.1.

For the  $L_3$  shell, the experimental and semiclassical cross sections generally agree within 10%, except in the adiabatic region  $\xi < 0.4$  where the cross-section ratios exhibit distinct maxima. The intensities and positions of the maxima vary with  $Z_2$  in a way similar to the  $L_2$  case, but the intensities of the maxima are lower. The results from the coupled-channel calculations in Fig. 5 show a maximum for Sn only, which may denote deficiency of the present model. However, we may not neglect the possibility that the maxima are generated by the averaging procedure [33,34] as the ECPSSR cross sections are overestimated in this region.

In all three subshells the cross-section ratios obtained by the coupled-channel calculation (Fig. 5) appear to be 10% lower than the ratios between the experimental and semiclassical cross sections in Fig. 4. We can immediately exclude the wave function effect as a possible reason since the cross section ratios for DHS wave functions (Fig. 1) are even higher than those of Fig. 4. The second source of the difference may be the uncertainty of the data base for the conversion of the x-ray production cross sections to ionization cross sections [33], which uses the radia-

tive widths of Scofield [36] and the Coster-Kronig and fluorescence yields of Krause [37]. Replacing the compilation [37] by the theoretical DHS data of Chen *et al.* [38], ionization cross sections generally 15% lower were obtained [33,39]. Lower experimental values imply lower cross section ratios of Figs. 1–4, as supported by Fig. 5.

The influence of the target electrons on the projectile kinematics may also contribute to the difference between the ratios in Figs. 4 and 5. As our targets were heavy atoms with a large number of electrons, the projectile effectively moved in the combined field of the nucleus and electron cloud. A simple correction procedure for the projectile motion suggested by [40,41] is to increase the projectile energy by the difference of the electron cloud potential. Expanding the screening function  $\chi$  up to the linear term, the correction term is independent of  $r$  and we find for the Firsov potential

$$\Delta V = \frac{Z_1 Z_2 e^2}{4\pi\epsilon_0 a_F} |\chi'(0)| = 48.73 Z_1 Z_2 \left( Z_1^{\frac{2}{3}} + Z_2^{\frac{2}{3}} \right)^{\frac{1}{2}} \text{ eV.} \quad (9)$$

The values of  $\Delta V$  were between 9 and 18 keV for our

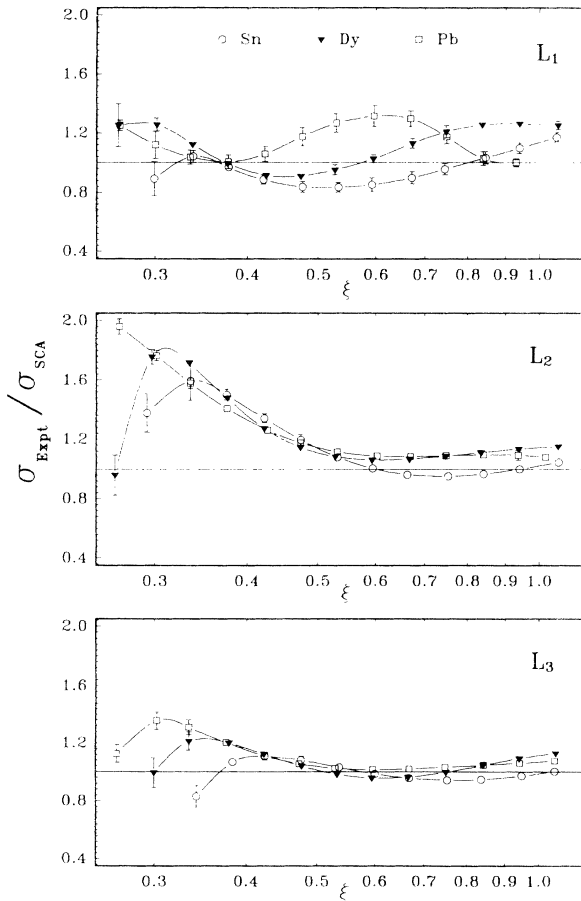


FIG. 4. The ratios between the average experimental and semiclassical cross sections, obtained by the present code which employs the hydrogenic Dirac wave functions according to the principle of Bethe.

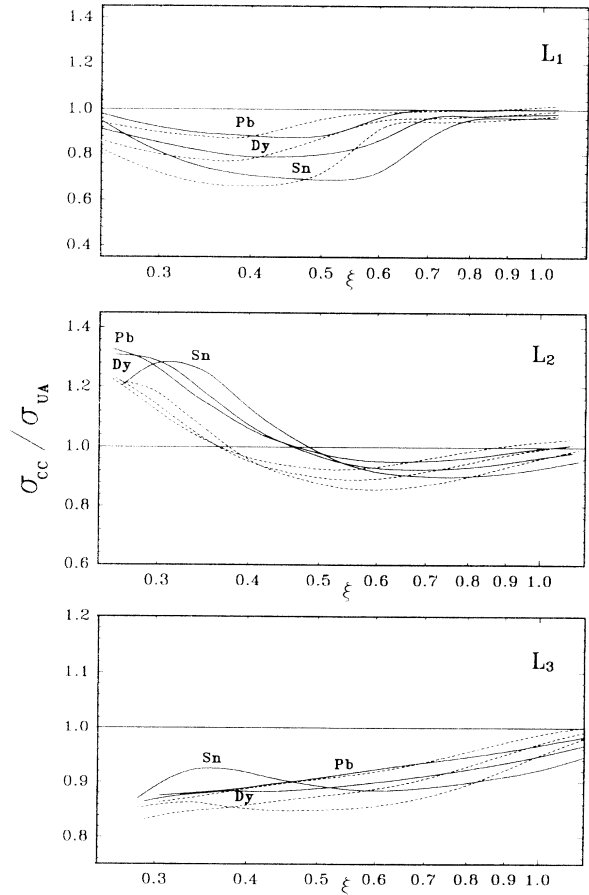


FIG. 5. The ratios between the cross sections obtained by the coupled-channel method and by the first-order calculation in the united-atom limit. The single final state is represented by the  $4s,p$  (solid line) or  $3s,p$  (dotted line) virtually bound state.

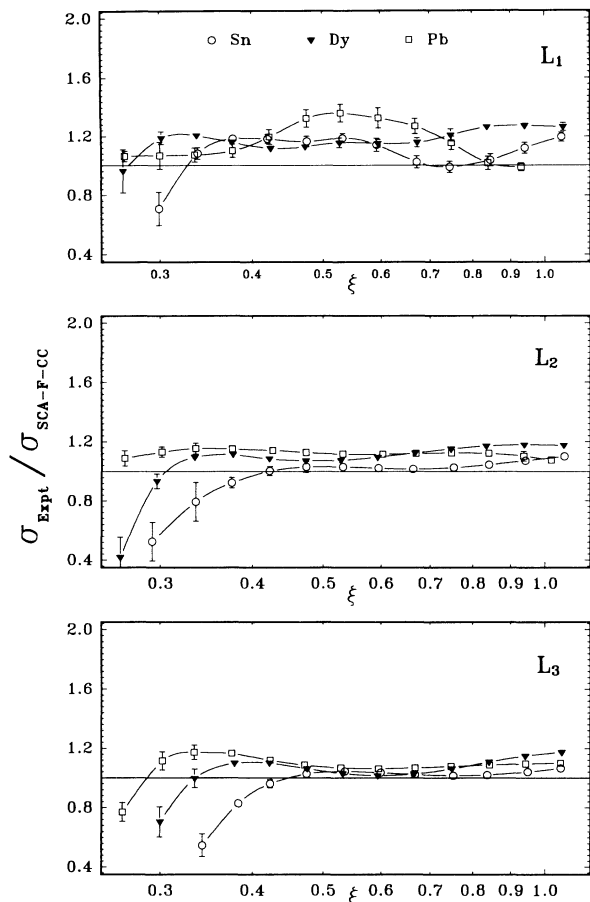


FIG. 6. The ratios between the average experimental and semiclassical cross sections, calculated for the proton energy increased by the difference of the electron cloud potential (9). The semiclassical cross sections are multiplied by the ratios of Fig. 5 to account for the intershell coupling.

targets and resulted in the cross sections being larger by 1% at  $\xi = 1$ , and by 5% at  $\xi = 0.6$ . The correction had a remarkable effect for  $\xi < 0.4$ , increasing the cross section by a factor of 2 at  $\xi = 0.3$ . The corrected SCA cross sections were multiplied by the ratios in Fig. 5 to account for the intershell coupling effect, and used for the normalization of the experimental data in Fig. 6. The resulting cross-section ratios approach a constant for a large part of the  $\xi$  interval, except in the very adiabatic region where the theoretical data exceed the experiment. The effect is larger for lighter elements which can be explained by an overestimated correction of the proton en-

ergy by the electron cloud potential. For the very adiabatic collisions, the ionization process occurs at internuclear distances close to the  $K$ -shell radius, for which the statistical description of the electron cloud is not valid.

For the  $L_1$  subshell, the relative intensity of the Pb peak is largely reduced and it is now comparable to the variation of the data for Sn and Dy. Figure 6 also shows that the experimental data exceed the theoretical cross sections by 10% for the  $L_{2,3}$  subshell and by 20% for the  $L_1$  subshell. This effect supports our previous statement that the data base of Scofield and Krause [36, 37] yields cross sections which are overestimated by several percent. Replacing the hydrogenic wave functions with DHS ones would result in the theoretical ionization cross sections being lowered by 10% for the  $L_{2,3}$  subshells and up to 20% for the  $L_1$  subshell. For  $L_1$ , the ratios between the experimental and theoretical cross sections could be up to 30% larger than unity. This is in accordance with the fluorescence yield uncertainty which is largest for the  $L_1$  subshell. Further refinements of the fluorescence and Coster-Kronig yield data base are beyond the scope of the present paper and may be found in [25,42,43].

## V. CONCLUSION

Among the different first-order theories, the semiclassical method which uses hydrogenic wave functions in the united-atom limit and obeys the principle of Bethe was found to be most efficient in reproducing the  $L$ -shell cross sections in a wide energy interval. Experimental and theoretical cross sections generally agree within 10–20%, except for the  $L_1$  subshell and  $L_{2,3}$  subshells in the velocity range  $\xi < 0.4$  where the intershell coupling strongly increases the cross sections. This phenomenon was confirmed by a simple coupled-channel model. The calculation also suggests that the ratio between the experimental and theoretical cross sections should be lower by 10%. Neither the use of the DHS wave functions nor the correction of the projectile kinematics for the outer electron screening can explain this difference. It is most probably due to the uncertainty of the fluorescence and Coster-Kronig yields used in the cross-section evaluation procedure.

## ACKNOWLEDGMENTS

The work was partly supported by Grant No. P1-0109-106 of the Slovenian Ministry of Science and Technology.

[1] I. Orlić, C.H. Sow, and S.M. Tang, *At. Data Nucl. Data Tables* **56**, 159 (1994).  
 [2] I. Orlić, *Nucl. Instrum. Methods Phys. Res. Sect. B* **87**, 285 (1994).  
 [3] W. Brandt and G. Lapicki, *Phys. Rev. A* **23**, 1717 (1981).  
 [4] H. Paul and J. Muhr, *Phys. Rep.* **135**, 47 (1986).  
 [5] Ž. Šmit, *Z. Phys. D* **22**, 411 (1991).  
 [6] T. Mukoyama and L. Sarkadi, *Phys. Rev. A* **25**, 1411 (1982).

[7] G. Basbas, W. Brandt, and R. Laubert, *Phys. Rev. A* **17**, 1655 (1978).  
 [8] E. Laegsgaard, J.U. Andersen, and M. Lund, in *Proceedings of the Tenth International Conference on Physics of Electron and Atomic Collisions, Paris, 1977*, edited by G. Watel (North-Holland, Amsterdam, 1977).  
 [9] J.U. Andersen, E. Laegsgaard, and M. Lund, *Nucl. Instrum. Methods Phys. Res.* **192**, 79 (1982).  
 [10] D. Trautmann and Th. Kauer, *Nucl. Instrum. Methods*

- Phys. Res. Sect. B **42**, 449 (1989).
- [11] Ž. Šmit, Phys. Rev. A **46**, 1367 (1992).
  - [12] M. Vigilante, P. Cuzzocrea, N. De Cesare, I. Murolo, E. Perillo, and G. Spadaccini, Nucl. Instrum. Methods Phys. Res. Sect. B **51**, 232 (1990).
  - [13] L. Sarkadi and T. Mukoyama, Nucl. Instrum. Methods Phys. Res. Sect. B **4**, 196 (1984).
  - [14] M.H. Chen and B. Crasemann, At. Data Nucl. Data Tables **33**, 217 (1985); **41**, 257 (1989).
  - [15] H.A. Bethe, in *Quantentheorie*, edited by H. Geiger and K. Scheel, Handbüch der Physik Vol. 24/1 (Springer-Verlag, Berlin, 1933), p. 273.
  - [16] D. Trautmann and F. Rösel, Nucl. Instrum. Methods Phys. Res. **214**, 21 (1983).
  - [17] E. Merzbacher and H.W. Lewis, in *Corpuscles and Radiation in Matter II*, edited by S. Flügge, Handbüch der Physik Vol.34 (Springer-Verlag, Berlin, 1958), p. 166.
  - [18] B.H. Choi, Phys. Rev. A **4**, 1002 (1971).
  - [19] J.D. Talman, J. Comput. Phys. **29**, 35 (1978).
  - [20] L. Kocbach, Z. Phys. A **279**, 233 (1976).
  - [21] P.A. Amundsen, J. Phys. B **11**, 3197 (1978).
  - [22] J. Bang and J.M. Hansteen, K. Dan. Vidensk. Selsk. Mat. Fys. Medd. **31**, No. 13 (1959).
  - [23] A.L. Ford, E. Fitchard, and J.F. Reading, Phys. Rev. A **16**, 133 (1977).
  - [24] L. Sarkadi and T. Mukoyama, Nucl. Instrum. Methods Phys. Res. Sect. B **61**, 167 (1991).
  - [25] L. Sarkadi and T. Mukoyama, Phys. Rev. A **37**, 4540 (1988).
  - [26] L. Sarkadi and T. Mukoyama, J. Phys. B **23**, 3849 (1990).
  - [27] M. Kregar, Physica C **113**, 249 (1982).
  - [28] I.C. Legrand, A. Berinde, C. Ciortea, A. Enulescu, D. Fluerașu, I. Piticu, V. Zoran, and H. Schmidt-Böcking, Nucl. Instrum. Methods Phys. Res. Sect. B **56/57**, 21 (1991).
  - [29] P.A. Amundsen and D.H. Jakubaša-Amundsen, J. Phys. B **21**, L99 (1988).
  - [30] K. Finck, W. Jitschin, and H.O. Lutz, J. Phys. B **16**, L409 (1983).
  - [31] L. Sarkadi, J. Phys. B **19**, 2519 (1986).
  - [32] W.H. Press, B.P. Flannery, S.A. Teukolsky, and W.T. Vetterling, *Numerical Recipes in C* (Cambridge University, Cambridge, England, 1988).
  - [33] C.H. Sow, M.S. thesis, National University of Singapore, 1993.
  - [34] I. Orlić (unpublished).
  - [35] N. De Cesare, F. Murolo, E. Perillo, D. Spadaccini, and M. Vigilante, Nucl. Instrum. Methods Phys. Res. Sect. B **83**, 325 (1993).
  - [36] J.H. Scofield, At. Data Nucl. Data Tables **14**, 121 (1974).
  - [37] M.O. Krause, J. Phys. Chem. Phys. Ref. Data **8**, 307 (1979).
  - [38] M.H. Chen, B. Crasemann, and H. Mark, Phys. Rev. A **24**, 177 (1981).
  - [39] E. Braziewicz, J. Braziewicz, T. Czyżewsky, L. Głowacka, M. Jaskóła, Th. Kauer, A.P. Kobzev, M. Pajek, and D. Trautmann, J. Phys. B **24**, 1669 (1991).
  - [40] G. Lapicki and W. Losonsky, Phys. Rev. A **20**, 481 (1979).
  - [41] A. Jakob, D. Trautmann, F. Rösel, and G. Baur, Nucl. Instrum. Methods Phys. Res. Sect. B **4**, 218 (1984).
  - [42] J.Q. Xu, Phys. Rev. A **43**, 4771 (1991).
  - [43] J.Q. Xu and X.J. Xu, J. Phys. B **25**, 695 (1992).